JOURNAL OF MAGNETIC RESONANCE, Series A **117,** 118–122 (1995)

COMMUNICATIONS

Frequency-Domain Analysis of Spin Motion Using Modulated-Gradient NMR

PAUL T. CALLAGHAN* AND JANEZ STEPIŠNIK†

**Department of Physics, Massey University, Palmerston North, New Zealand; and †J. Stefan Institute, University of Ljubljana, Ljubljana, Slovenia*

Received June 19, 1995; revised July 27, 1995

In pulsed-gradient spin-echo NMR, one measures the displacement of nuclear spins over the time interval, Δ, between two gradient pulses, of duration δ and amplitude g, placed in the dephasing and rephasing evolution periods of a spin-echo RF pulse sequence. For sufficiently narrow gradient pulses, the experiment is nicely described in terms of a scattering wave-vector formalism so that the echo amplitude is inherently acquired in a time–wave-vector domain as

$$E(q, \Delta) = \int_{-\infty}^{\infty} \bar{P}(Z, \Delta)\exp(-i2\pi qZ)\,dZ, \qquad [1]$$

where $q = (2\pi)^{-1}\gamma g\delta$ and $\bar{P}(Z, \Delta)$ is the averaged propagator describing the probability that a spin will displace by Z along the direction of the magnetic field gradient over the time Δ.

The PGSE NMR technique suffers from the limited time window available for the study of nuclear spin motion. Δ is limited above by the available nuclear-spin relaxation time and below by the need to apply sufficient gradient pulse area (i.e., q) in the available time Δ between the pulses. Indeed, at the lower limit, the ability to apply these pulses with a duration sufficiently narrow to retain the propagator description of the motion becomes severely curtailed. In practice, Δ is generally required to be in excess of a few milliseconds for this condition to apply.

An entirely different viewpoint to the measurement of motion using magnetic field gradients has been proposed by Stepišnik (*1, 2*). In this approach, one treats the effect of the gradient via the time dependence of the accumulated spin phase. It turns out that the natural description of the spin motion is via the velocity auto-correlation function, rather than via the propagator for displacement. Furthermore, it may be shown that the spectral density of this translational velocity auto-correlation is ''probed'' by a sampling function given by the frequency spectrum of the time integral of the effective gradient waveform. Indeed, the mathematical treatment lends itself to analogy (*3*) with the measurement of rotational dipolar auto-correlation spectral density via the ''probe'' of the spin relaxation times, where T_1 samples at positions ω_0 and $2\omega_0$, while $T_{1\rho}$ samples at ω_1 and $2\omega_1$.

The purpose of the present Communication is to demonstrate an implementation of the frequency-domain analysis using two different modulation waveforms for the effective gradient. We term this method *f*requency-*d*omain analysis of spin motion using *m*odulated-*g*radient *NMR* (FD-MG-NMR). We note that the use of oscillating gradients to probe molecular motion has been recently reported by Wang *et al.* (*4*). That approach, originally suggested in Refs. (*1–3*), suffers from the influence of a strong zero-frequency lobe which dominates the sampling of the motional spectrum. We demonstrate here an idealized modulation waveform which delivers a sampling of the translation motion spectrum in a manner most akin to a delta function at frequency, ω.

The detailed theory of the generalized treatment of modulated gradients has been given elsewhere (*1–3, 5*), and we simply sketch the important points. We shall assume a general (uniform) modulation effective-gradient waveform, $\mathbf{G}(t)$, noting the 180° RF pulses have the effect of inverting the sign of prior gradients in the usual manner. Provided one is dealing with stochastic spin motion in which sudden local phase changes are avoided, it is possible to show that the ensemble phase distribution arising from such motion is Gaussian in character and that the (normalized) echo attenuation at time t may be written

$$E(t) = \sum_i \exp[i\theta_i(t) - \beta_i(t)], \qquad [2]$$

where the $i\theta_i(t)$ is a phase shift arising from molecular flow or drift while $\beta_i(t)$ is an attenuation factor which arises from random particle migration. We shall be particularly concerned with this latter effect. It should be noted that the sum is taken over the spin subensembles which are sufficiently small to represent the distribution of sample boundary conditions and sufficiently large for the local density matrix to be evaluated and a local spin magnetization described.

1064-1858/95 $12.00

The evaluation of the sum over i is subtle in the case of restricted diffusion and the ensemble average should not be transferred to the exponent without careful justification. This is a delicate point which we are not concerned to address in this paper. Instead, we shall deal with cases where such an average is justified and note that

$$\theta(t) = \int_0^t [\mathbf{F}(t) - \mathbf{F}(t')]\cdot\langle \mathbf{v}_{is}(t')\rangle dt' \qquad [3a]$$

and

$$\beta(t) = \tfrac{1}{2}\int_0^t \int_0^t \mathbf{F}(t')\langle \mathbf{v}_{is}(t')\mathbf{v}_{is}(t'')\rangle \mathbf{F}(t'')dt'dt'', \quad [3b]$$

where

$$\mathbf{F}(t) = \gamma \int_0^t \mathbf{G}(t')dt'. \qquad [4]$$

$\mathbf{F}(t)$ is zero at the time of spin-echo rephasing. This property enables the use of *per partes* integration when evaluating the spin phase and hence the derivation of Eq. [3] in terms of the spin velocity rather than the spin displacement. Noting that the spectral density of the ensemble-averaged velocity auto-correlation function is simply the diffusion tensor

$$\mathbf{D}(\omega) = \int_0^\infty \tfrac{1}{2}\langle \mathbf{v}_{is}(t')\mathbf{v}_{is}(0)\rangle \exp(i\omega t')dt', \qquad [5]$$

we may write

$$\beta(t) = \frac{1}{\pi}\int_0^\infty \mathbf{F}(\omega)\mathbf{D}(\omega)\mathbf{F}(-\omega)d\omega \qquad [6]$$

which simplifies, in the case of isotropic diffusion, to

$$= \frac{1}{\pi}\int_0^\infty \mathbf{D}(\omega)|\mathbf{F}(\omega, t)|^2 d\omega. \qquad [7]$$

The gradient-modulation spectrum, $\mathbf{F}(\omega)$, is given by

$$\mathbf{F}(\omega) = \int_0^t \mathbf{F}(t')\exp(i\omega t')dt'. \qquad [8]$$

In Fig. 1, we show three alternative gradient-modulation waveforms and their associated spectra. It is clear that the third of these waveforms, involving a repetitive CPMG train of RF pulses with interspersed gradient pulses, produces the nearly ideal frequency sampling function. We refer to the time-domain/frequency-domain characteristics of this sequence as single-lobe/ac. It should be noted that the ''ideal'' ac form of Fig. 1c could be also achieved by means of a constant background gradient. We prefer to use the pulsed version shown in order to minimize slice-selection effects associated with the hard 180° pulses being applied in the presence of a background gradient.

By contrast, the oscillating gradient waveform shown in Fig. 1a has a dominant zero-frequency lobe which hinders the sampling of the spectral density at variable frequencies. This zero-frequency lobe is associated with the dc offset in the time integral of the effective gradient, whereas waveform three is appropriately centered. Consequently, we refer to such a sequence as having double-lobe/dc character. Such a ''dc offset'' effect can be produced with the CPMG train by positioning the gradient pulses slightly differently (as shown in Fig. 1b).

The dominant sampling lobe of the idealized sequence is at $\omega = 2\pi/T$ and has width of order $1/NT$. With $N \geqslant 4$, a reasonably narrow peak can be achieved as seen in the calculated spectra shown in Fig. 1. In principle, it is possible to use such a sequence to probe spectral densities in the frequency range 10 Hz to 100 kHz. This becomes possible because rather than using two gradient pulses, for which the attenuation effect disappears as the gradient pulse duration, δ, is shortened, the repetitive pulse train employs an increasing number of gradient pulses in any time interval t, as the frequency is increased and T is reduced. Thus, the frequency-domain analysis extends downward the effective time scale of the PGSE experiment to the submillisecond regime.

The total area under the two lobes of the gradient spectrum differs by a factor of three between waveforms 1b and 1c. The expected echo attenuation factors are respectively given by

$$\beta \approx \tfrac{1}{2}NT\gamma^2G^2\delta^2[2\mathbf{D}(0) + \mathbf{D}(2\pi/T)]$$
$$(\text{''dc/double-lobe'' sequence}) \qquad [9]$$

and

$$\beta \approx \tfrac{1}{2}NT\gamma^2G^2\delta^2\mathbf{D}(2\pi/T)$$
$$(\text{''ac/single-lobe'' sequence}). \qquad [10]$$

We are able to test Eqs. [9] and [10] by applying the sequence to the measurement of spin-echo attenuation in pure water for which the diffusion spectrum is practically flat out to terahertz frequencies. We expect the slopes of $\log(E)$ vs NT to be frequency independent and to differ by a factor of three in the case of the two sequences.

To this end, we have implemented waveforms 1b and 1c on a Bruker AMX300 spectrometer using a specially constructed quadrupole gradient coil of sensitivity 1.13 T m^{-1} $Å^{-1}$. Using short gradient pulses of amplitude 6.78 T m^{-1}, with effective (i.e., area equivalent) pulse durations δ of 70 μs and with the interval between gradient pulses $(T/4)$ ranging between 150 and 1200 μs ($\omega/2\pi$ = 1.67 to

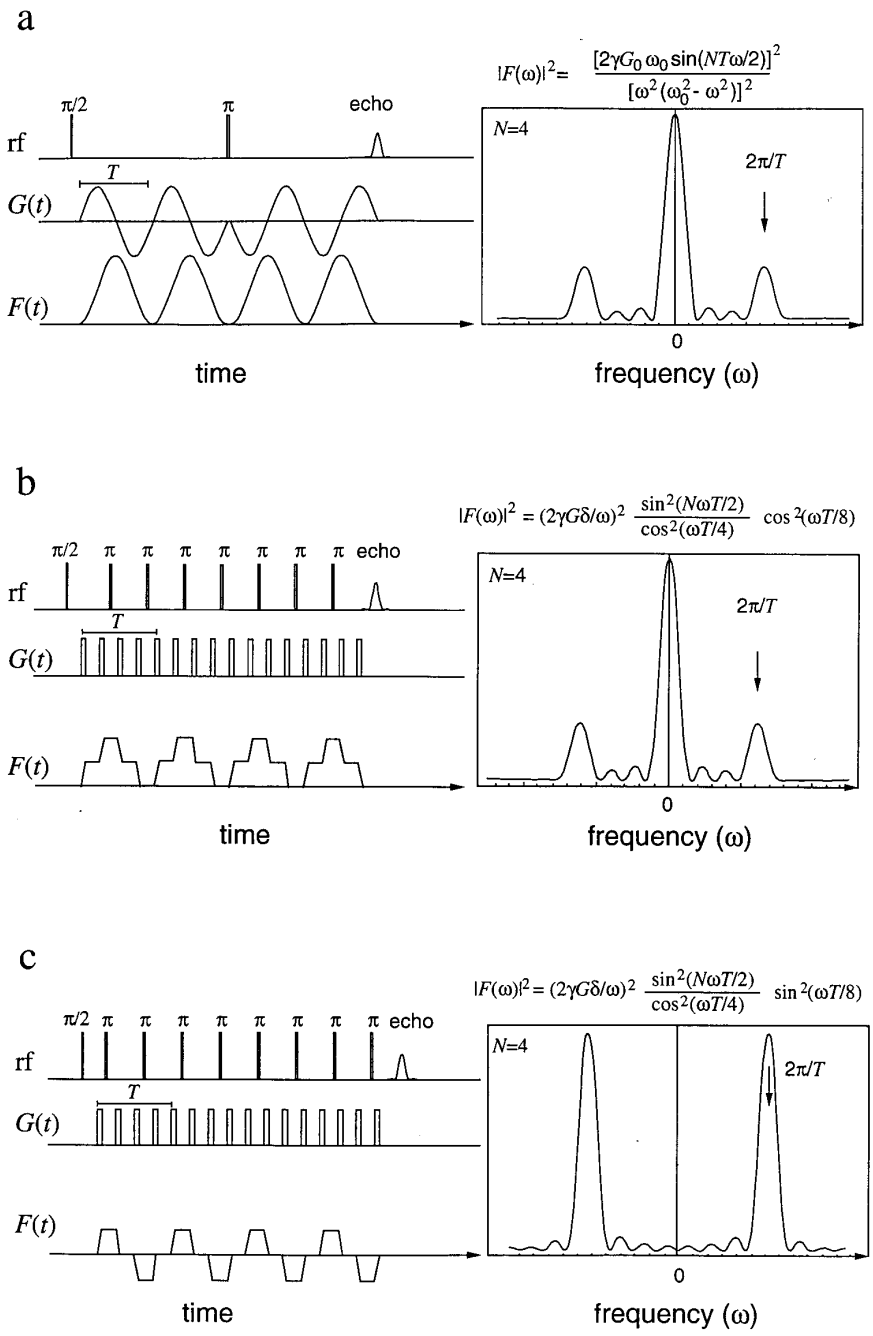

FIG. 1. FD-MG NMR RF and gradient pulse sequences, showing the (actual) gradient modulation waveform $G(t)$, the time integral of the effective gradient waveform, $F(t)$, and the square of the spectrum of $F(t)$. $|F(\omega)|^2$ directly samples the diffusion spectrum via the integral expressed in Eq. [7]. In the spectral equations ω_0 is $2\pi/T$ while G_0 and G are amplitudes of the sinusoidal and pulse gradient waveforms, respectively. The waveforms and spectra are for (a) sinusoidal gradient modulation, (b) double-lobe/dc rectangular modulation, and (c) single-lobe/ac rectangular modulation. Note that pulse sequence (c) samples the diffusion spectrum at a single frequency and therefore represents the ideal probe of the diffusion spectrum.

0.21 kHz), we obtained the results shown in Fig. 2a. Note that we have performed the experiment by varying N at fixed gradient amplitude, G. Before plotting the exponential decays, we eliminate the effect of T_2 relaxation by normalizing with data obtained in an equivalent experiment but with zero gradient.

The slopes are indeed independent of frequency except for the highest frequency where a small reduction in slope is found due to the effect of finite pulse rise time and consequent deviation from ideal rectangular time integral, $F(t)$. Within experimental error, the slopes in each case differ between the ac and dc waveforms by the predicted factor of

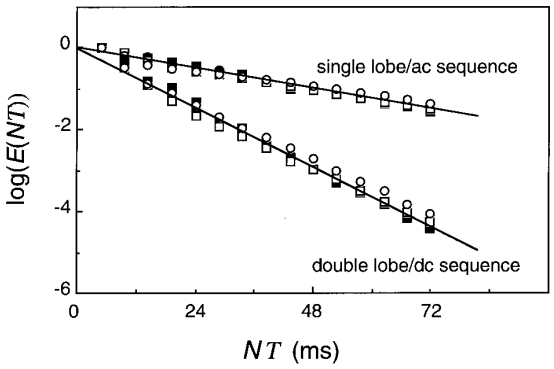

FIG. 2. Echo-attenuation plots for pure water at room temperature, obtained using pulse sequences 1b (double lobe/dc) and 1c (single lobe/ac) for four different values of τ (150, 300, 600, and 1200 μs) corresponding to sampling frequencies of 1667, 833, 417, and 208 Hz respectively. The gradient pulse amplitude was 6.78 T m^{-1} with effective (i.e., equivalent square pulse) duration 70 μs. The lines correspond to Eqs. [9] and [10] and the known diffusion coefficient of water. Note that the highest-frequency data exhibit a somewhat reduced value of β because of the effect of finite pulse rise time.

three and are consistent with the known diffusion coefficient of water.

The system we have chosen in order to provide a translational motion spectral density of sufficient complexity comprises a close-packed stack of ion-exchange beads around which water flows in the manner shown in Fig. 3. The motion depicted can be represented in terms of three superposed and uncorrelated velocity components as

$$\nu(t) = \nu_0(t) + \nu_1(t) + \nu_2(t), \qquad [11]$$

where $\nu_0(t)$ represents the local microscopic Brownian fluctuation, $\nu_1(t)$ is the coherent curvilinear flow around the beads, while $\nu_2(t)$ represents the perfusive spreading motion. To first order, $\nu_1(t)$ can be described by the function $aV\cos(\Omega t + \theta)$ where Ω is the angular velocity of the fluid around the beads, V is the local fluid speed, while the phase angle θ is random across the bead pack. The attenuation factor a takes account of the need to consider the component of fluid velocity along the direction of the applied gradient. The local fluid speed V is related to the volume flow rate Q, the capillary radius R, and the (effective) local water volume fraction ϕ, by $V = Q/\pi R^2\phi$, while Ω is given by V/r where r is the local bead radius.

The auto-correlation function of $\nu_1(t)$ in the vicinity of a bead of radius r is therefore $\frac{1}{2}a^2V^2\cos[\Omega(r)t]$. Both $\nu_0(t)$ and $\nu_2(t)$ are incoherent motions albeit on vastly different time scales. Their velocity autocorrelation functions can be represented by the simple exponential forms, $\overline{\nu_0^2}\exp(-t/\tau_0)$ and $\overline{\nu_2^2}\exp(-t/\tau_2)$. The microscopic Brownian correlation time, τ_0, is given by $D_0/\overline{\nu_0^2}$ where D_0 is the self-diffusion coefficient of free water, while the perfusion correlation time, τ_2, is expected to be on the order of $\Omega(r)^{-1}$. It is easy to show that the total velocity auto-correlation function and its spectral density are given by

$$\begin{aligned}\langle\nu(t)\nu(0)\rangle &= (D_0/\tau_0)\exp(-t/\tau_0) \\ &\quad + \tfrac{1}{2}a^2V^2\int_0^\infty P(r)\cos(Vt/r)\,dr \\ &\quad + \overline{\nu_2^2}\int_0^\infty P(r)\exp(-tV/r)\,dr \qquad [12]\end{aligned}$$

and

$$\begin{aligned}\mathbf{D}(\omega) &= \frac{D_0}{1+\omega^2\tau_0^2} + \tfrac{1}{2}a^2V^2\int_0^\infty P(r) \\ &\quad \times\left[\tfrac{1}{2}\delta(\omega - r/V) + \tfrac{1}{2}\delta(\omega + r/V)\right]dr \\ &\quad + \overline{\nu_2^2}\int_0^\infty P(r)\,\frac{r/V}{1+\omega^2r^2/V^2}\,dr. \qquad [13]\end{aligned}$$

Assuming a Gaussian distribution of bead sizes with standard deviation, σ [i.e., $P(r) = (2\pi\sigma^2)^{-1/2}\exp(-(r-r_0)^2/2\sigma^2)$] and noting that $\omega\tau_0 \ll 1$ for all practical values of ω, we find that

$$\begin{aligned}\mathbf{D}(\omega) &= D_0 + \tfrac{1}{4}a^2V^2(V/\omega^2)(2\pi\sigma^2)^{-1/2} \\ &\quad \times\exp[-(V/\omega - r_0)^2/2\sigma^2)] \\ &\quad + \overline{\nu_2^2}\int_0^\infty P(r)\,\frac{r/V}{1+\omega^2r^2/V^2}\,dr. \qquad [14]\end{aligned}$$

Figure 4a shows the translational spectral density measured for water flowing through a column of ion-exchange resin (AG1108, BioRad, Richmond, California), comprising beads of 50–100 mesh. These were packed in a capillary of 2.0 mm inner diameter and the magnetic field gradient pulses

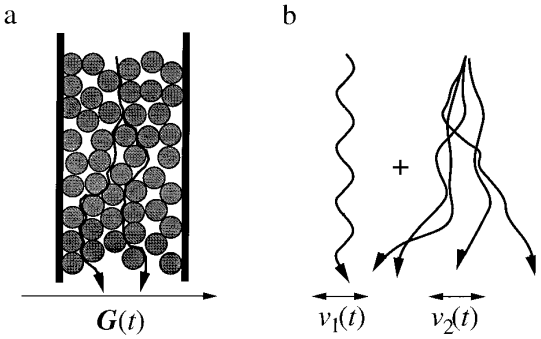

FIG. 3. (a) Simplified model of velocity for fluid traveling through a bead pack. (b) Decomposition of the motion into an oscillatory part, $v_1(t)$, and a perfusive spreading, $v_2(t)$. Both are superposed on the microscopic Brownian motion, $v_0(t)$. Note that the transverse component is measured in our experiment.

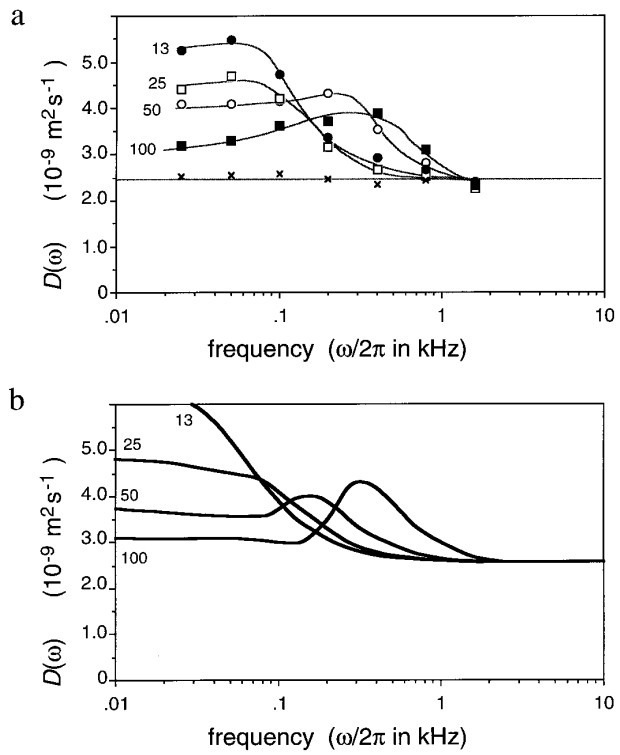

FIG. 4. (a) Diffusion spectra for water traveling through ion-exchange-resin bead pack at flow rates of 13 ml h^{-1} (solid circles), 25 ml h^{-1} (open spares), 50 ml h^{-1} (open circles), and 100 ml h^{-1} (solid squares). The crosses represent the measured spectrum for stationary water. The lines are to guide the eye. (b) Theoretical predictions based on Eq. [14]. A common set of parameters is used to generate the set for differing flow rates.

were applied normal to the average flow direction. The water flow was controlled using a reciprocating piston (Pharmacia P500) pump, and flow rates were varied between 13 and 100 ml h^{-1}. For these experiments the same single-lobe/ac pulse train was used as in the water experiments but with waveform frequencies varying in factors of two between 1666.7 and 20.8 Hz, providing a frequency range of nearly two orders of magnitude. This was implemented using a gradient amplitude of 4.52 T m^{-1} (with effective pulse area width 60 μs) while NT was varied up to 600 ms using $T/4$ values between 150 μs and 9.6 ms. Values of N were sufficiently high for $|\mathbf{F}(\omega)|^2$ to be considered a delta function at cyclic frequency $1/T$.

The resulting spectra exhibit a characteristic peak at a frequency which shifts downward as the water speed is decreased. The spectra for all flow rates reach a common high-frequency plateau of D_0 and have a low-frequency plateau which increases with decreasing fluid velocity. All these features are represented by Eq. [14], and to demonstrate this, a set of theoretical curves generated using the equation is shown for comparison in Fig. 4b. The only adjustable parameters (which are common to the set of four curves) are a, ϕ, and ν_2^2 which were set to 0.017, 0.025, and 3×10^{-6} m^2 s^{-2}, respectively.

As a result of this model we may ascribe the following explanation to the translational spectral density shown in Fig. 4a. The low-frequency plateaus arise from the slow perfusive random walk, the peaks correspond to the coherent motion associated with fluid in curvilinear motion around the beads, and the high-frequency plateaus arise from the microscopic Brownian (self-diffusive) motion. These clearly defined features are a direct consequence of the sharp, single-lobed frequency profile associated with the FD-MG-NMR sequence shown in Fig. 1c. It is clear that this waveform represents an almost ideal probe of the motion spectrum. We contend that such a waveform is superior to those whose time integrals retain a dominant zero-frequency lobe, such as the simple oscillating gradient suggested in our earlier theory (*1–3*).

The application demonstrated here suggests that frequency-domain modulated-gradient NMR is a technique of great utility, especially when the time integral of the effective gradient waveform has the optimized spectrum. In particular, it provides fresh insight regarding the problem of perfusion, enabling a clear separation of motion over differing time scales. In principle, the method can be applied to the study of restricted diffusion in porous media and to the elucidation of internal mode dynamics of large polymers. The theoretical treatments which reveal the spectral density for such systems are not at all straightforward (*6*), and these treatments, along with experimental applications of FD-MG-NMR is such systems, will be the subject of future investigations.

ACKNOWLEDGMENTS

We are grateful to Dr. Ross Mair for making us aware of the existence of Ref. (*4*) and to Dr. Eiichi Fukushima for making available a copy of his ENC poster. Funding support from the New Zealand Foundation for Research, Science, and Technology is gratefully acknowledged.

REFERENCES

1. J. Stepisnik, *Physica B* **104,** 350 (1981).
2. J. Stepisnik, *Prog. NMR Spectrosc.* **17,** 187 (1985).
3. P. T. Callaghan, ''Principles of Nuclear Magnetic Resonance Microscopy,'' Oxford Univ. Press, Oxford, 1991.
4. L. Z. Wang, S. A. Altobelli, D. O. Kuethe, and E. Fukushima, 36th ENC, Poster 547, Boston, 1995.
5. J. Stepisnik, *Physica B* **198,** 299 (1994).
6. P. T. Callaghan and J. Stepisnik, ''Advances in Magnetic and Optical Resonance,'' in press, 1996.